NASA TN D-1526

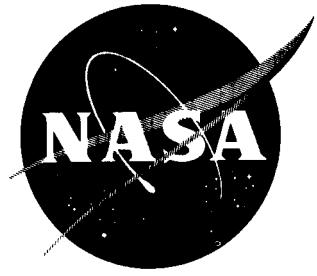

TECHNICAL NOTE

D-1526

A CONSIDERATION OF LUNAR SURFACE BALLISTICS AND THE HAZARDS ASSOCIATED WITH SPACECRAFT LANDING OR LAUNCH OPERATIONS

By D. C. Cramblit

George C. Marshall Space Flight Center
Huntsville, Alabama

NATIONAL AERONAUTICS AND SPACE ADMINISTRATION
WASHINGTON
March 1963

TABLE OF CONTENTS

LIST OF ILLUSTRATIONS

NATIONAL AERONAUTICS AND SPACE ADMINISTRATION

TECHNICAL NOTE D-1526

A CONSIDERATION OF LUNAR SURFACE BALLISTICS AND THE HAZARDS ASSOCIATED WITH SPACECRAFT LANDING OR LAUNCH OPERATIONS

By

D. C. Cramblit

SUMMARY

With the advent of lunar landings planned for the near future, it is essential that considerable though be given to the behavior of jet exhaust in a vacuum under low gravity conditions, especially in relation to the most probable lunar surface conditions. Of primary concern is the motion of lunar surface particles resulting from the impingement of exhaust gases from a lunar landing or takeoff space vehicle and the resulting hazards to the vehicle itself and to both local and distant manned lunar bases or facilities. The combined parameters of low gravity, high vacuum, and high energy exhaust gases result in the displacement of large masses over considerable distances, so that the problem is not merely a localized one.

This preliminary study was directed specifically toward determination of the trajectories or flight paths of lunar surface particles accelerated by the jet blast from a lunar landing or return vehicle. A range of particle velocities was assumed based on an anticipated effective exhaust gas velocity of 13,250 ft/sec for a LOX-LH_2 engine. Thus, velocities both above and below those required for escape or orbit from the lunar surface were considered. Data are presented in graph and chart form, along with a brief discussion. Sample calculations and basic data for the ballistics study are presented in Appendix I. Appendix II describes in detail the follow-on work to be accomplished and the problems to be encountered in an analysis aimed at predicting the mass and distribution of particles most likely to be associated with the velocity range assumed in Appendix I. Determination of the momentum energy relationships between exhaust gases and lunar surface particles of assumed sizes and density will give us a better feel for the degree of hazard involved.

As discussed later in Section II and Appendix II, large dust clouds, and the ballistics of relatively large lunar surface particles resulting from a lunar landing or return launching may present serious problems in

relation to the landing operation itself and most definitely can produce hazardous conditions for both distant and surrounding lunar base facilities, equipment, and personnel.

Of course, more studies will be required in these areas when more definitive data on the exact composition and structure of the lunar surface is obtained. Such studies will be needed to provide data upon which to base lunar facility design concepts and operational criteria.

SECTION I. DISCUSSION OF RESULTS

It was considered reasonable to assume that lunar surface particles would attain velocities ranging from 0 to 8000 ft/sec when subjected to the exhaust of a LOX-H_2 engine with an effective exit velocity of 13,250 ft/sec, considering that some velocity energy will be lost in transmission through standoff shock waves and through deflection from the lunar surface. Since the escape velocity from the lunar surface is 7800 ft/sec and the circular orbital velocity is 5540 ft/sec, one can readily envision that escape, orbiting of particles, or extremely eccentric partial orbits may occur as a result of exhaust jet impingement. Appendix I contains sample calculations and a summary of data (Tables I, II, and III) for a number of assumed initial particle velocities and initial angles with respect to the local vertical. The varying angles were considered because of assumed erosion of the lunar surface with time during jet impingement. Test data in Reference 1 includes that this pattern will be in the form of a conic section, with a final semi-vertex angle of approximately 50 degrees.

Figure 1 shows the hyperbolic flight path for a particle accelerated to a velocity greater than escape. For assumed velocities of 7410 ft/sec and 6350 ft/sec, which are less than escape velocity, Figures 1 and 2 apply. The velocities exceed circular orbital velocity at the lunar surface so that an eccentric orbit is possible. However, here we note the stringent requirements for an orbit initiated from the lunar surface. Assuming the particle has an initial velocity exceeding the circular orbital velocity, then the initial launch point would be the low point or perigee of a hypothetical orbit. Also since it is launched from the surface instead of at some altitude, the takeoff angle with respect to the local vertical would necessarily be exactly 90 degrees in order that an orbit be possible. The possibility of an orbit is further restricted in that the initial particle impulse would necessarily have to take place from a very high point so that the particle would not impact on a nearby hillside or other obstruction prior to traveling over the horizon and attaining or orbit. Thus, with a firing angle of 90 degrees and a velocity greater than circular velocity, one complete orbit is possible but highly improbable. At any angle other than 90 degrees, eccentric partial orbits resulting in long surface ranges would be experienced. Figures 1 and 2 describe the flight paths for initial velocities of 7410

and 6350 ft/sec and number of assumed angles with respect to the local vertical. Figure 3 depicts the actual lunar surface range covered by these same particles. Of course, for the departure angle of zero degrees from the horizontal, the theoretical distance given is equivalent to one orbit or, more precisely, the circumference of the moon.

For assumed velocities less than circular orbital velocity, figure 4 applies. In this case, conic section central force field ballistic equations taking into account the moon s curvature were utilized in determining the resulting particle ranges (Appendix I). Figure 5 describes particle range based on velocities from 88 to 550 ft/sec and as defined by standard ballistic equations neglecting curvature.

Preliminary conclusions arrived from following this analysis will be discussed in the following section.

SECTION II. RECOMMENDATIONS AND CONCLUSIONS

A review of the data indicating the ranges attained by objects as a function of initial velocity leads one to conclude that depending upon surface composition, a lunar landing or return operation may result in the bombardment of both local and distant lunar bases with relatively large size particles. This is especially evident under the existing lunar conditions of vacuum, low gravity, and high energy exhaust gases.

Such bombardment could prove hazardous to facilities, associated equipment, and personnel, especially where lightweight inflatable thin film strucutes or shelters are proposed. These problems must be considered in the siting and design of future lunar facilities so that adequate protection will be provided.

Jet impingement may also result in the formation of large dust clouds covering a considerable area of the lunar surface, thus proving hazardous to the landing operation. Coverage of large surface areas is expected becuase of jet expansion effects resulting from the gross under-expansion of jet nozzles in a vacuum. As shown from data of a preliminary test data in a vacuum (Appendix II), cratering will occur upon jet impingement on a "soft" lunar surface. If the scale model tests conducted by Lewis are any indication, the "cratering" from a full scale LOX-LH_2 nozzle will be quite sizeable and will present a formidable design problem in developing a safe lunar landing system. Of course, all of this is based on assumed lunar surface conditions which may or may not exist. Initial unmanned landings will probably clarify this aspect of the problem.

Because of the critical nature of these problems, it is concluded that additional study work should be directed toward determination of the particle masses that will most probably be accelerated to the range

of velocities just studied. This, of course, would necessarily be based on a range of assumed particle densities. The general approach to the future study work to be performed is discussed in Appendix II. It will first be necessary to determine the overpressures at the deflecting surface as a function of nozzle height above the surface, propellant type, and nozzle characteristics, such as operating chamber pressure, and available gas stream momentum energy must be related in parametric equations predicting probable particle motion. For both phases of the problem, and especially Part 2 (as discussed more fully in Appendix II) a considerable amount of additional test work is required. This is necessary because the variable particle velocity factor cannot be separated in an equation from the other time-dependent variables without making a number of assumptions based on the existing supply of inadequate test data.

APPENDIX I - SAMPLE CALCULATIONS

BASIC LUNAR DATA

R = Radius of Moon = 1082 miles

W = Angular rotation = 1 rev/27.33 earth days

Surface Velocity at Equator = 10.4 miles/hr

$g_{moon} = 1/6\ g_{earth} = 5.37\ ft/sec^2$

$M_m = Mass_{moon} = \frac{1}{81.375}\ Mass_{earth}$

$Mass_{earth} = 6.595 \times 10^{21}$ tons

G = Universal gravitational force constant = $\frac{3.44 \times 10^{-8}\ ft^4}{lb\text{-}sec^4}$

PROPULSION DATA

Assume that the orbital launch or landing vehicle is propelled by two $LOX\text{-}LH_2$ engines, rated at 15,000 lb thrust each.

Assume I_{sp} of these engines in vacuum = 412 sec

Propellant flow/engine = $\frac{Thrust}{I_{sp}} = \frac{15,000}{412} = 36.5$ lb/sec

For both engines, total gas flow = 73 lb force/sec

Effective Exhaust Velocity = $I_{sp}\ (g_{earth})$

= 412 sec (32.2 ft/sec^2) = 13,250 ft/sec

Based on this exhaust velocity, potential escape, orbit, and ballistic flight paths of lunar surface particles must be considered. A sample calculation for various assumed velocities will now be presented.

Case 1 - $V_{initial}$ > escape velocity

$V_{escape\ from\ moon} = \sqrt{\frac{2\ GM}{r}}$

G = universal gravitational constant

M = Mass of moon

r = distance from center of moon to point of injection = R_{moon}

V_{escape} = 7800 ft/sec at the lunar surface

Since the assumed particle velocity exceeds the escape velocity at the lunar surface, it will escape from the moon and fall toward the earth for any angle of B_o sufficient to clear local obstacles (Fig. 1).

Case 2 - Assume velocity = 6350 ft/sec

The initial velocity of this particle, 6350 ft/sec, is less than escape velocity but more than the velocity required for a circular orbit at the lunar surface.

$$V_{\text{circular orbit}} = \sqrt{\frac{g\ R^2_{moon}}{r_{orbit}}} \simeq 5540 \text{ ft/sec}$$

Since the initial particle velocity does exceed the orbital velocity, an orbit is potential with the low point or perigee being the point of takeoff. A potential orbit can also be verified by reference to the equation defining λ on Figure 6.

$$\lambda = \frac{V_o^2\ r_o}{GM} = \frac{V_o^2}{g\ r_o} \text{ where } GM = g\ r_o^2$$

λ is a parameter equivalent to twice the ratio of kinetic to potential energy of the particle at takeoff and is also equal to

$$\left(\frac{V_{actual}}{V_{\text{reqd for circular orbit}}}\right)^2$$

Therefore, if λ is = > 1, the local velocity is higher than circular orbital velocity, and an orbit is potential.

For the case of V = 6350 ft/sec,

$$\lambda = \frac{(6.35)^2 \times 10^6 \text{ ft}^2 \text{ sec}^2}{\text{sec}^2\ 5.37 \text{ ft } (1.082 \times 10^3)\ (5.28 \times 10^3)\ \frac{\text{ft}}{\text{mile}}\ \text{mile}}$$

$$= 1.315$$

$\therefore$, satellite orbit is possible, depending on angle of injection.

If angle B_o is 90 degrees, the eccentricity of a potential orbit is defined by

$$e = \sqrt{1 - \lambda (2 - \lambda) \sin^2 B_o}$$

$$e = \sqrt{1 - 1.315 (2 - 1.315) (1)} = \underline{0.316}$$

Flight paths are defined by the following (Fig. 7):

$e < 1$ - elliptical

$e = o$ - circular

$e = 1$ - parabolic

$e > 1$ - hyperbolic

$\therefore$ elliptical equations apply.

The apogee of the potential orbit is defined by $r_{max.} = \frac{1 + e}{2 - \lambda} (r_o)$ where r_o in this case = radius of injection from lunar centroid = R_{moon} apogee or $r_{max.} = \frac{1.316}{0.685}$ (1082) = 2080 miles, or 1000 miles above the lunar surface.

$$\text{Radius of perigee} = \frac{1 - e}{2 - \lambda} (r_o) = 1 (R_{moon}) = R_{moon}$$

Therefore, if B_o is 90 degrees and the particle is initially launched from a high point on the lunar surface, it could conceivably make one complete orbit before impact. As could be expected, however, the possibility of an orbit is practically nil because of the stringent requirements.

It can be shown that for angles of B_o less than 90 degrees calculated perigee point is less than the radius of the moon so that no orbit is possible. To determine the actual range covered on the lunar surface (Fig. 7).

r, which is shown as the distance to a point on the elliptical path is defined by the equation

$$r = \frac{p}{1 + e \cos \alpha}$$

p is the semilatus rectum of the ellipse $= \frac{b^2}{a} = \frac{V_o^2 \sin^2 B_o}{g_o} = a(1-e^2)$

α is the angle measured from the perigee to a point on the elliptical path (Fig. 7).

The value of r as a function of e,p, and cos α then defines the elliptical path. In considering potential orbits, by letting r = R of the moon, angle α indicates the angle from the perigee to a point on the elliptical path a distance equal to the moon's radius from the foci. To have an orbit, angle α must be 0 degrees. Any angle of α greater than 0 degrees indicates that the perigee radius of the theoretical elliptical orbit is less than the radius of the moon, which, of course, makes a closed orbit impossible. For example, consider the case for V_o = 7410 ft/sec. By firing horizontally, (B = 90 degrees), P = 1940 miles, and e = 0.79,

$$r = \frac{p}{1 + e \cos \alpha}$$

where $r = R_{moon}$, $\cos \alpha = \frac{1}{e}\left[\frac{p}{R} - 1\right] = \underline{\therefore \alpha = 0° \text{ (or } 360°)}$

This indicates that the point of particle take-off from the lunar surface is the perigee of the orbit, and an orbit could occur if the particle did not hit any local obstructions prior to traveling over the local horizon (Fig. 1).

It can be shown that for any angle of B_o less than 90 degrees, a complete orbit is not possible. Consider V_o = 7410 ft/sec with B = 30 degrees.

$$p = \frac{b^2}{a} = \frac{V_o^2 \sin^2 B_o}{g} = \frac{(7.41)^2 \times 10^6 (0.25)}{5.37} = 2.56 \times 10^6 \text{ ft}$$

$$e = \text{eccentricity} = \sqrt{1 - \lambda (2 - \lambda) \sin^2 30°} = 0.952$$

$$\text{let } r = R_{moon} = 5.7 \times 10^6 \text{ ft}$$

$$r = \frac{p}{1 + e \cos \alpha}$$

$$\alpha = \cos^{-1}\left[\frac{1}{e}\left(\frac{p}{r} - 1\right)\right] \quad \text{for } [\quad] > 0$$

$$\alpha = \pi - \cos^{-1}\left[\quad\right] \text{ for } \left[\quad\right] > 0$$

$$\alpha = 125.45°$$

Thus, no orbit is possible. Since the point of departure from the lunar surface remains constant, this indicates that the hypothetical perigee of the ellipse and the major axis of the ellipse has shifted an angle α of 125.45 degrees with respect to the ellipse where B = 90 degrees. (Fig. 1, axis shift from x-x to z-z). Since the ellipse is symmetrical, the impact point on the opposite side of the axis will also be defined by angle α, and the angular range covered on the lunar surface by the partial orbit will be defined by 360 degrees - 2 α.

For this case, the surface range(s) is defined as follows:

$$(s) = R_{moon}\ (d\ \theta) = R_{moon}\ \frac{(360 - 2\ \alpha)}{180}\ \pi$$

$$(s) = 1082 \text{ miles} \left[\frac{360-2\ (125.45)}{180}\right] \pi = 2060 \text{ miles.}$$

After determing the axis shift for each angle of departure (B), the relationships established above were utilized in plotting the flight paths shown in Fig. 1 and 2 for velocities of 7410 and 6350 ft/sec (See Fig. 3 also).

Case 3 - Assume V = 4040 ft/sec (Fig. 4)

An initial velocity of 4040 ft/sec is less than escape or orbital velocity. Also, λ is considerably less than 1. Therefore, ballistic range equations are applicable. As given by Fried & Richardson (Ref. 1), the range angle θ (the circular angle transversed by the object from launch to impact) is given by the following equation:

$$\theta = 180 - \sin^{-1}\left[\frac{(1 - \sigma\lambda \sin^2 B_o)}{(1 - 2\lambda \sin^2 B_o + \lambda^2 \sin^2 B_o)^{\frac{1}{2}}}\right] - \text{Tan}^{-1}\left[\frac{1-\lambda \sin^2 B_o}{\sin B \cos B}\right]$$

where $\sigma = 1 + \frac{h^*}{R}$

*h is defined as the altitude at burnout. In our case, which is identical to impulsive burning or instantaneous application of all thrust at the lunar surface, h = 0. $\therefore$ $\sigma = 1$

The range from take-off to impact may also be defined as follows:

$$\text{Range} = \frac{2\,R_{moon}}{} \tan^{-1}\left[\frac{V_o^2 \sin B_o \cos B_o}{R_{moon}\, g_{moon} - V_o^2 \sin^2 B_o}\right]$$

For $B_o = 75°$

$$\text{Range} = 5.7 \times 10^6 \text{ ft } (2) \tan^{-1}\left[\frac{(4.04)^2 \times 10^6\ (0.9659)\ (0.2588)}{30.6 \times 10^6 - (4.04)^2 \times 10^6\ (0.934}\right]$$

$\tan^{-1} = 0.266 = 14.9°$

$$\therefore \text{Range} = \frac{11.4 \times 10^6 \text{ ft} \quad \text{mile} \quad 14.9\ \pi}{5280 \text{ ft} \quad 180} = \underline{560 \text{ miles}}$$

A similar approach was taken for other angles of B and for reduced velocities. When the range became very short ($V < 1000$ ft/sec) the use of basic ballistic equations neglecting curvature was found acceptable (Fig. 5).

PERIOD OF REVOLUTION-ELLIPTICAL ORBITS

The period of revolution (Figs. 1 and 2) of the hypothetical particle orbits where the initial velocity exceeded orbital velocity is defined by the following equation:

$$T = \sqrt{\frac{4\,\pi^2\,a^3}{\mu}}$$

where $a = \frac{p}{1 - e^2}$ (Fig. 7)

and μ = gravitational factor = gR^2

g = gravitational pull - ft/sec^2

R = radius from center of lunar mass to orbit

Data for all of the above referenced figures is summarized in Tables I, II, and III.

TABLE I. LUNAR BALLISTICS DATA

Init. Velocity (Ft/sec)	Angle of Departure with Local Horizontal	Flight Data
8400	Any angle sufficient to clear local obstructions	Follows a hyperbolic path to escape.
7410	0°	Complete orbit possible Range 6800 miles Maximum ht above lunar surface at apogee = 8150 miles
	15°	Lunar surface range = 5560 miles Maximum ht at apogee = 8220 miles
	30°	Maximum ht at apogee = 8430 miles Surface Range = 4300 miles
	45°	Maximum ht at apogee = 8720 miles Surface range = 3160 miles
	60°	Maximum ht at apogee = 10,070 miles Surface range = 2060 miles
6350	0°	Orbit possible Maximum ht above lunar surface at apogee = 1000 miles Perigee = r_{moon}
	15°	Maximum ht at apogee = 1130 miles Surface range = 4760 miles
	30°	Maximum ht = 1400 miles Maximum range = 3360 miles
	45°	Maximum ht = 1660 miles Maximum range = 2370 miles
	60°	Maximum ht = 1890 miles Maximum range = 1525 miles

TABLE II. RANGE VERSUS ANGLE OF DEPARTURE DATA

Init. Velocity (Ft/sec)	Range (Miles) Vs. Angle of Departure with Local Horizontal				
	0°	15°	30°	45°	60°
V_o = 4040	0	560	795	750	560
2870		194	313	332	268
1800		64	109	120	102
1200		25.4	44	51	44
900		14.3	24.8	28.6	24.8
616		6.7	11.6	13.4	11.6
600		6.35	11	12.7	11
550		5.35	9.25	10.7	9.25
500		4.4	7.64	8.8	7.64
400		2.82	4.89	5.65	4.89
300		1.59	2.75	3.18	2.75
200		0.7	1.22	1.41	1.22
100		0.174	0.306	0.353	0.306
88		0.137	0.237	0.274	0.237

TABLE III. FLIGHT PATH DATA (V_o > CIRCULAR ORBITAL VELOCITY)

V_o = 7410 ft/sec

B (Degrees)	α (Degrees)	e	p (Miles)	r (Miles)	e cos α	cos α
	20			1110	0.741	0.94
90	45	0.790	1940	1245	0.559	0.707
			1940	1940	0	0
	90		1940			
	135		1940	4400	-0.559	-0.707
	180		1940	9240	-0.79	-1.0
	225		1940	4400	-0.559	-0.707
	270		1940	1940	0	0
	315		1940	1245	+0.559	+0.707
	360		1940	1082	+0.79	+ 1
75 (Axis shift 32.85)	20	0.805	1810	1030	0.756	
	45		1810	1150	0.570	
	90		1810	1810	0	
	135		1810	4120	-0.570	
	180		1810	9290	-0.805	
	225		1810	4210	-0.570	
	270		1810	1810	0	
	315		1810	1510	+0.570	
	360		1810	1000	+0.805	
	20	0.847	1455	810	0.796	
60	45		1455	910	0.60	

TABLE III. FLIGHT PATH DATA (V_o > CIRCULAR ORBITAL VELOCITY) (Cont'd)

V_o = 7410 ft/sec

B (Degrees)	α (Degrees)	e	p (Miles)	r (Miles)	e cos α	cos α
	90		1455	1455	0	
	135		1455	3640	-0.6	
(Axis Shift 66)	180		1455	9500	-0.847	
	225		1455	3640	-0.6	
	270		1455	1455	0	
	315		1455	910	+0.6	
	360		1455	788	+0.847	
45	20	0.900	970	526	0.845	
(Axis Shift 96.55)	45		970	594	0.636	
	90		970	970	0	
	135		970	2660	-0.636	
	225		970	2660	-0.636	
	270		970	970	0	
	315		970	594	+0.636	
	360		970	510	0.9	
30	20	0.952	485	256	0.895	
(Axis Shift 125.45)	45		485	290	0.673	
	90		485	485	0	
	135		485	1485	-0.673	
	180		485	10,000	-0.952	
	225		485	1485	-0.673	

TABLE III- FLIGHT PATH DATA (V_o > CIRCULAR ORBITAL VELOCITY) (Cont'd)
V_o = 7410 ft/sec

B (Degrees)	α (Degrees)	e	p (Miles)	r (Miles)	e cos α
	270		485	485	0
	315		485	290	+0.673
	360		485	248	+0.952

TABLE III - FLIGHT PATH DATA (V_o > CIRCULAR ORBITAL VELOCITY) (Cont'd)

V_o = 6350 Ft/sec

B (Degrees)	α (Degrees)	e	p (Miles)	r (Miles)	e cos α
90	20	0.316	1420	1095	0.297
	45		1420	1160	0.224
	90		1420	1420	0
	135		1420	1830	-0.224
	180		1420	2080	-0.316
	225		1420	1830	-0.224
	270		1420	1420	0
	315	0.316	1420	1160	+0.224
	360		1420	1080	+0.316
75 (Axis Shift 55)	20	0.400	1330	966	0.376
	45		1330	1035	0.283
	90		1330	1330	0
	135		1330	1855	-0.283
	180		1330	2220	-0.4
	225		1330	1855	-0.283
	270		1330	1330	0
	315		1330	1035	+0.283
	360		1330	950	+0.4
60 (Axis Shift 91.2)	20	5.700	1065	695	0.535
	45		1065	759	0.403
	90		1065	1065	0
	135		1065	1780	-0.403

TABLE III- FLIGHT PATH DATA (V_o > CIRCULAR ORBITAL VELOCITY) (Cont'd)

V_o = 6350 ft/sec (Cont'd)

B (Degrees)	α (Degrees)	e	p (Miles)	r (Miles)	e cos α
	180		1065	2480	-0.57
	225		1065	1780	-0.403
	270		1065	1065	0
	315		1065	759	+0.403
	360		1065	679	+0.57
45	20	0.742	713	420	0.697
(Axis Shift 117.25)	45		713	467	0.525
	90		713	713	0
	135		713	1500	-0.525
	180		713	2760	-0.742
	225		713	1500	-0.525
	270	0.742	713	713	0
	315		713	467	+0.525
	360		713	409	+0.742
30	20	0.880	356	195	0.826
(Axis Shift 139.55)	45		356	220	0.622
	90		356	356	0
	135		356	941	-0.622
	180		356	2960	-0.88
	225		356	941	-0.622
	270		356	356	0
	315		356	220	+0.622
	360		356	189	+0.88

APPENDIX II

PROBLEM AREAS FOR FUTURE STUDY

This preliminary study has indicated the velocity ranges and ballistics to be encountered on blast accelerated lunar particles. The problem now remains to determine the masses of particles that will most probably be accelerated to these velocities. The problem of establishing the momentum energy transferred to these particles is fraught with many uncertanties and inseparable variables. With knowledge of exhaust gas densities, mass flow rates, stand-off shock wave theory, and gas velocity, one can determine the maximum over-pressure and resulting forces that could conceivable be initially applied to an object in the jet stream. Through knowledge of the initial temperature and flow rate of gases, the energy loss at impact, and the probable angles of deflection as a result of surface erosion, one can use a molecular approach to calculate the momentum energy within the gases per unit area of dispersion for a given distance or time and thus calculate the force that would be applied to a stationary object at that point. However, since the particle is in motion, the force, and of course the velocity and acceleration curves of the particle will be an integral function of time. In typical dimensional analysis, blast wave variables are determined as a function of time by four major parameters: (1) Shock over-pressure, (2) Ambient pressure, (3) Time duration of the positive winds and (4) The speed of sound in the undisturbed air. Of course, items (2) and (4) become zero under lunar conditions. Furthermore, it is soon realized that even for conditions such as that on earth, a completely pure mathematical solution is not possible because the variable particle velocity factor cannot be separated in an equation from the other time-dependent variables. For this reason, most blast effect equations here on earth are based on empirical relations determined by fitting curves to computed blast data (Ref. 2).

Practically all existing theory developed on secondary-missile behavior has come about as a result of weapons effect studies. Very often, semi-empirical relations are used to define over-pressure duration as a function of blast yield, over-pressure, ambient pressure, and the speed of sound. Then, with knowledge of the velocity of propagation of the pressure disturbance, the displaced object motion can be predicted. None of these analyses are adaptable to our problem, since there is not an instantaneous release of energy and there really is no wave or over-pressure propagation in a vacuum; there is only gas dispersion, the initial dispersion being a function of nozzle height above the lunar surface and the nozzle configuration or degree of under-expansion.

A review of nearly all of the listed references relating to blast or jet exhaust effects indicates that most work to date is based specifically on one type of rocket engine and one specific situation, and is not transposable to another engine or operating condition. This indication is also

brought out clearly in Ref. 3. What is really required in the follow-on study to this report is a breakdown of the problem into the following areas:

1. A determination of the over-pressure at the deflecting surface as a function of nozzle height above the surface, propellant type, and nozzle characteristics such as operating pressure, nozzle contour, and expansion ratio.

2. Definition of the relationships between surface over-pressures and momentum energy transfer to secondary particles. Because of the difficulties involved in a pure mathematical approach to Part 2, it appears that it will be necessary to implement basic parameteric equations with some test data and/or empirical relationships. Perhaps the first effort at obtaining such data was made by Lewis Research Center (Ref. 4) where recent tests were made in a vacuum to determine the pressure distributions and erosion patterns on simulated hard and soft lunar surfaces. These model tests were performed with cold air jets at nozzle pressure ratios up to 288,000. Some of the more important results of these tests were:

a. Surface pressure distributions were dependent on nozzle area ratio. For nozzles with area ratios ranging from 1 to 25, the nozzle total pressure ratio remained constant at 288,000. However, the nozzle static pressure ratio $P_{exit}/P_{ambient}$, which is an index of jet spreading, varied from 152,000 for a sonic nozzle ($A_{exit} = A_{throat}$) to 545 for a conical nozzle with an area ratio of 25 and a corresponding exit Mach number of 5. At the largest descent heights (approximately 40 throat diameters) the surface pressures were low and uniformly distributed with the sonic nozzle. As the conic nozzle area ratio was increased, at the same distance, the surface pressure also increased. However, with an area ratio of 25, the maximum surface pressure was only 0.3 percent of the chamber pressure. The shape of the pressure curves with decreasing valves of decent height was generally symmetrical, with the peak value on the jet centerline. A maximum surface pressure of 5 percent chamber pressure was recorded for the 25/1 conical nozzle at a descent height of 10 throat diameters. This nozzle had a throat diameter of 0.50 inch, an exit diameter up to 2.5 inch (expan. ratio = 25/1) and a maximum length from throat to exit of 3.75 inches.

b. Surface pressure distributions were also dependent on nozzle contour. Short bell-shaped nozzles gave annular surface pressure distributions as a result of shock coalescence originating within the nozzle.

c. The high pressure area on the simulated lunar surface was small in comparison with the diameter of the billowing jet. In general, the high pressures were contained within a circle whose diameter was about 16 throat diameters, regardless of area ratio or nozzle contour.

d. The surface pressures increased rapidly as the vehicle approached the simulated lunar surface. The maximum pressure at a descent height of 40 throat diameters was only 0.4 percent of the chamber pressure, but increased to 6 percent at 13 throat diameters.

Data from the above series of tests and hopefully, some future tests of a similar nature relating surface pressure to nozzle height above the surface, chamber pressure, and nozzle parameters will be utilized in Phase 1 of follow-on studies to establish equations relating these variables to the "effective" momentum energy available in the gas stream upon striking the lunar surface. Of course, this "effective" value will be less than the theoretical valve because of jet expansion effects and loss of kinetic energy in passage of the gas stream through the standoff shock wave.

In addition to the tests described above, Lewis Research Center conducted qualitative investigations in a 4 x 6 foot vacuum facility to visually explore the erosion caused by the impingement of an under-expanded jet on a thick layer of 0.010-inch-diameter, white-sand particles. "Cold air at a pressure of 150 pounds per square inch absolute was supplied to a small nozzle having a throat diameter of 1/32 inch and a corresponding weight flow of 0.00224 pound per second. A conical nozzle with an area ratio of 12 and contoured nozzles with area ratios of 150 and 500 were tested at descent heights ranging from about 200 to 600 throat diameters. The experimental runs lasted for 2.7 seconds, during which time the vacuum tank pressure increased from an initial value of 8×10^{-2} millimeter to 8×10^{-1} millimeter of mercury. Nozzle total-pressure ratio thus dropped from 100,000 to 10,000 during this cycle. Erosion patterns were recorded photographically through a glass window on one end of the tank".

"During the initial start of the flow from the nozzle a curious erosion pattern was obtained. The jet eroded an annular depression in the sand, while the central area remained intact. Surface erosion patterns of this type have also been observed from the downwash of VTOL aircraft. The erosion progressed toward the center with time; a central peak formed and projected briefly above the surface and then collapsed. This phenomenon, which generally occurred during the first 0.5 second, was more pronounced at the lower descent heights where the interior peak was higher and lasted longer. The jet continued to "dig" a large circular concave hole after the elimination of the central peak.

The final hole depth and diameter were recorded photographically, and the following general results were obtained:

1. Variations in nozzle area ratio from 12 to 500 had little measurable effect on either the depth or diameter of the hole.

2. As descent height decreased from 575 to 192 throat diameters, the hole diameter increased from 200 to 250 throat diameters while the depth remained essentially constant at about 60 throat diameters.

3. The sand particles were thrown upward and outward in a sheet forming essentially a conical surface with a semivertex angle that averaged about 50 degrees. However, since the particles apparently followed a ballistic trajectory, at no time did any of the sand strike the vehicle. Maximum particle heights were estimated to be about 480 throat diameters."

Result 1 above can be justified by taking a look at the test nozzle characteristics:

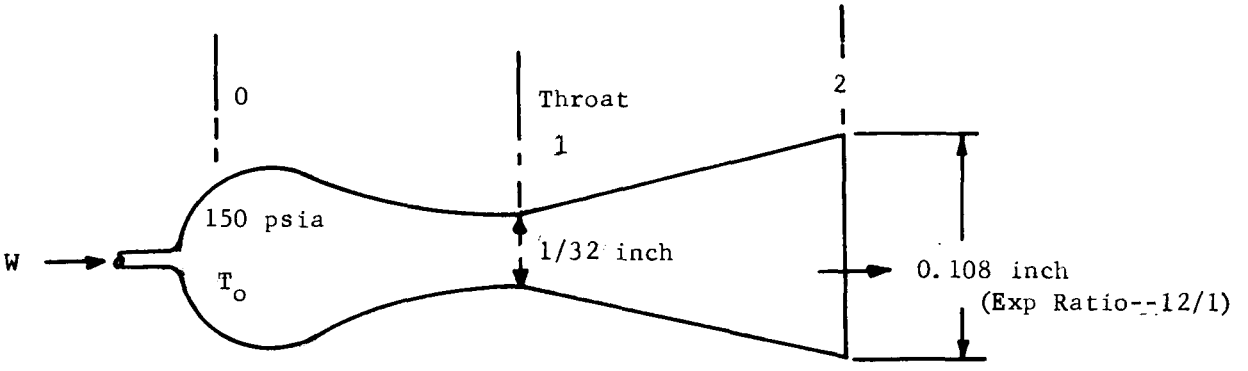

$W = 0.00224$ lb/sec

As given in Ref. 14, Equation 4.17,

$$\Gamma_o = \left(\frac{A^* P_o}{W}\right)^2 \frac{K}{R} \left(\frac{2}{K+1}\right)^{\frac{K+1}{K-1}}$$

where A^* = throat area

$P_o = 150$ psia

$W = 0.00224$

$K = 1.4$ for air

$R = 53.3$ ft lb f/lb_{mass} °R

$\therefore$ $T_o = 745°$ R

at a Mach number of unity,

$$T_1 = 0.8333\ (745) = 620^\circ\ R$$

$$P_1 = 0.528\ (150) = 79.3\ \text{psia}$$

$$\rho_o = \frac{150\ (144)}{53.3\ (745)} = 0.545\ \text{lb/ft}^3$$

$$\rho_1 = 0.634\ (\rho_o) = 0.345\ \text{lb/ft}^3$$

C_o = speed of sound at $T_o = \sqrt{KRT_o} = 1340$ ft/sec

$$\frac{C_1}{C_o} = \sqrt{\frac{T_1}{T_o}} = \sqrt{0.832} = 0.912$$

$C_1 = V_1 = 0.912\ (C_o) = 1220$ ft/sec velocity at Throat

using tables for compressible isentropic flow, the following was obtained:

For $A_2/A_1 = 12$ (Case 1)

$P_2 = 0.82$ psia

M = Mach No. = 4.133

$T_2 = 0.2258\ (T_o) = 168^\circ\ R$

$$M^* = 2.154 = \frac{V_2}{C^*} = C_1$$

$V_2 = 2.154\ (1220\ \text{ft/sec}) \cong$ 2620 ft/sec

For $A_2/A_1 = 500$ (Case 2)

$P_2 = 0.004155$ psia

M = 9.828

$T_2 = 36.8^\circ\ R$

$M^* = 2.388$

$V_2 = 2.388\ (1220) \cong$ 2920 ft/sec

Therefore, although the exit Mach numbers for the two cases vary considerably, the exit velocities change a very small amount. Thus, there is very little change in the kinetic energy of the exhaust gases and as such, nozzle area ratio variations would not be expected to cause much change in the "cratering" effect.

Result 2 indicates an increase in hole dia. from 6.25 to 7.8 inches when the nozzle was lowered from 18 to 6 inches. Diameter increase is attributable to increase surface pressure with a corresponding increase in kinetic energy transmitted/unit surface area; all as a result of reduced jet expansion effects at reduced heights above the surface. Very little change in depth may have been a result of compaction of the subsurface particles after initial impingement and also because of the increase in the test chamber pressure from 0.08 to 0.8 mm Hg during the 2.7-second test run. Such an ambient pressure increase could have materially affected the degree of energy transfer to the surface particles. Actually, this test data has practically no quantitative value because of lack of surface pressure distribution information. Also, test nozzles of the size used are very sensitive to flow variables and can very easily give erroneous or misleading test data in addition to being very difficult to obtain scaling factors for. It is apparent that much more test data taking into account all the dependent variables is required to enable future determination of particle motion parameters and cratering effects. This must be done by holding all variables constant but one until all combinations have been analysed.

Result 3 indicates that there will probably be no hazards to the vehicle as far as backflow of particles is concerned. A maximum particle height (0.01 inch dia. particle) of 480 throat diameters, assuming a departure angle of 50 degrees from the vertical (following the sides of the crater) is equivalent to an initial velocity of 14 ft/sec. Again, there is insufficient data to attempt a correlation of these results to other nozzle configurations. More testing is in order.

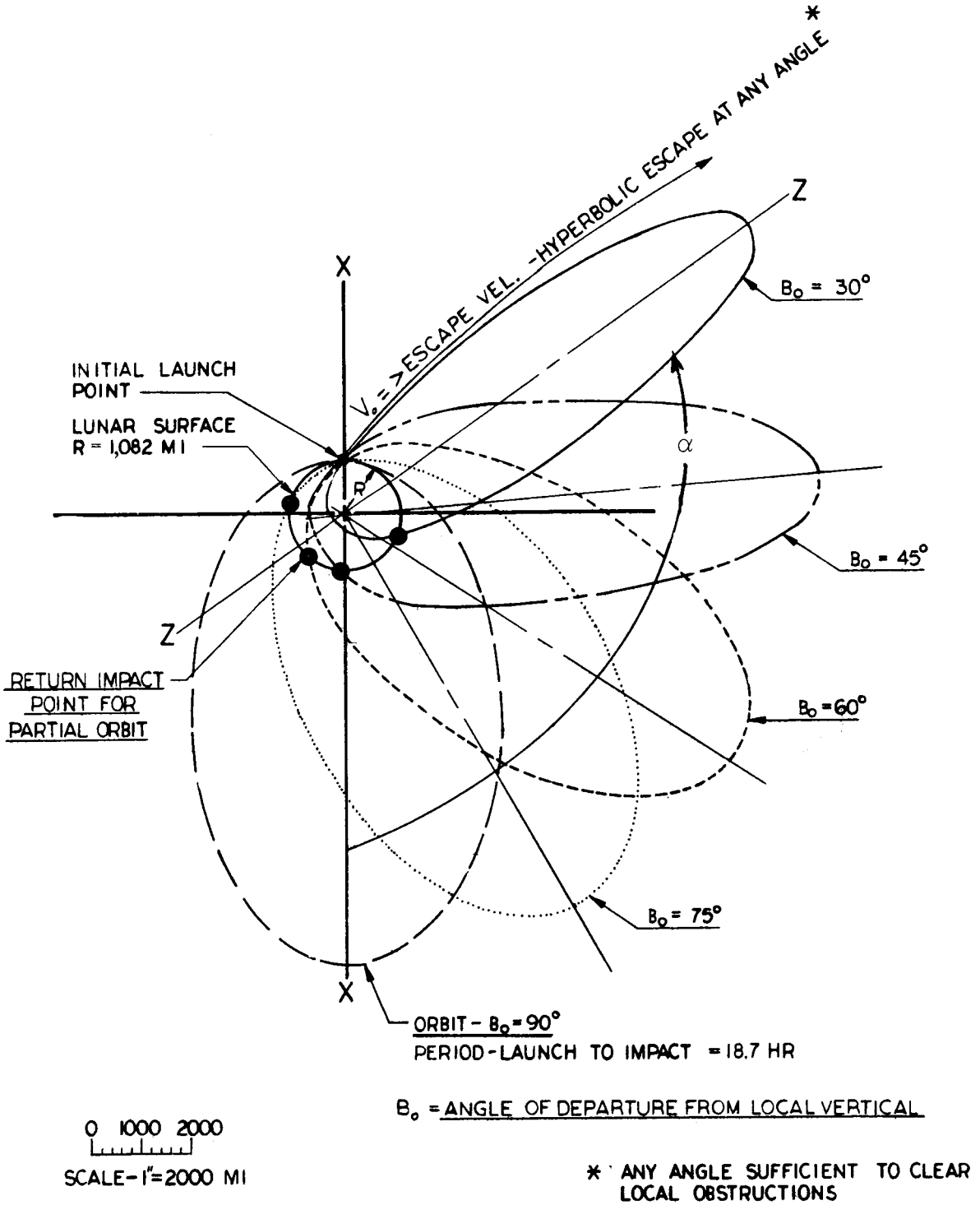

FIGURE 1. PARTICLE TRAJECTORIES $-V_o = V_{ESCAPE} - V_o = 7410$ FT/SEC.

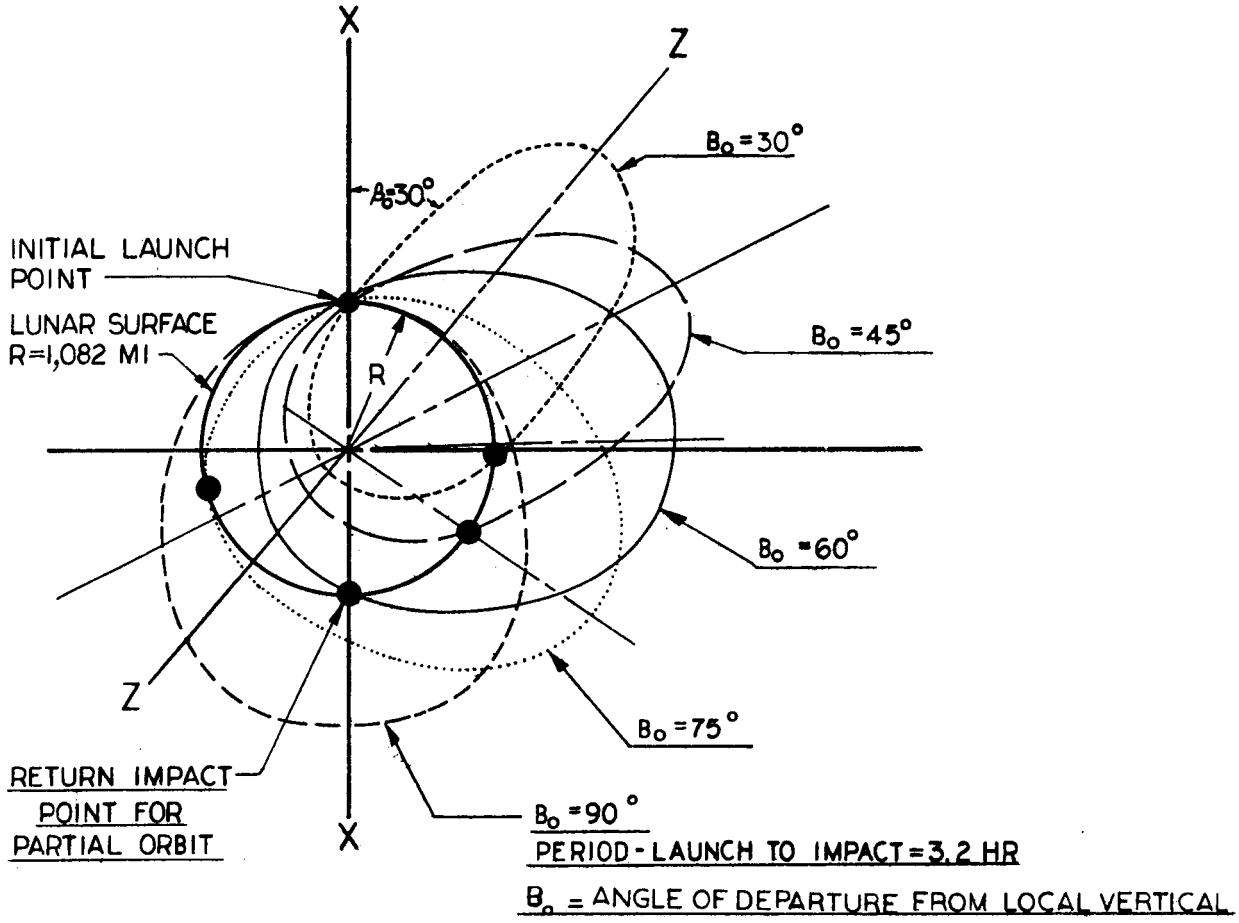

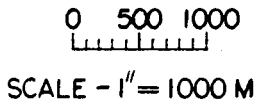

FIGURE 2. PARTICLE TRAJECTORIES - V_o = 6350 FT/SEC

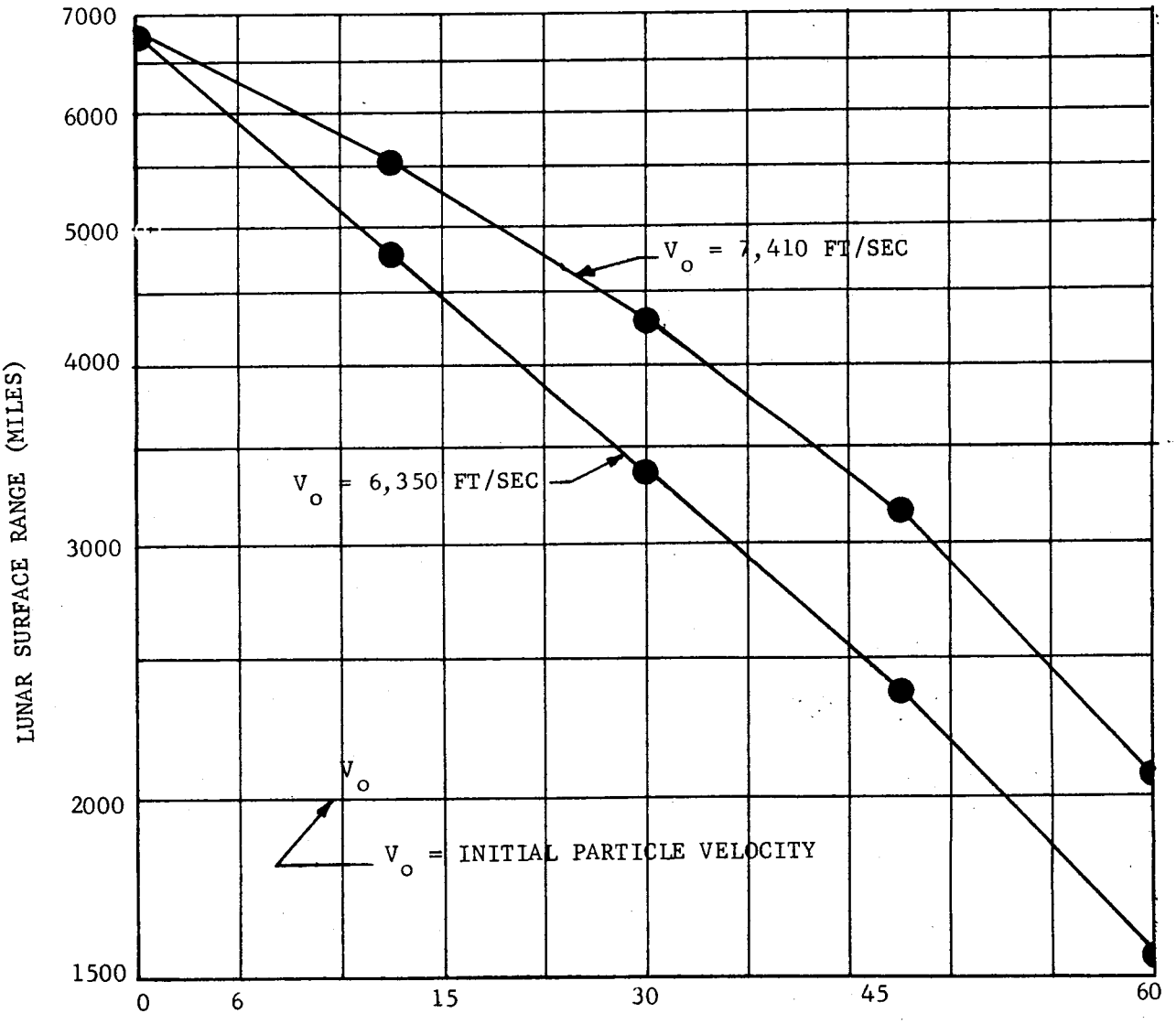

FIGURE 3. PARTICLE RANGE VERSUS ANGLE OF DEPARTURE V_o > CIRCULAR ORBITAL VELOCITY.

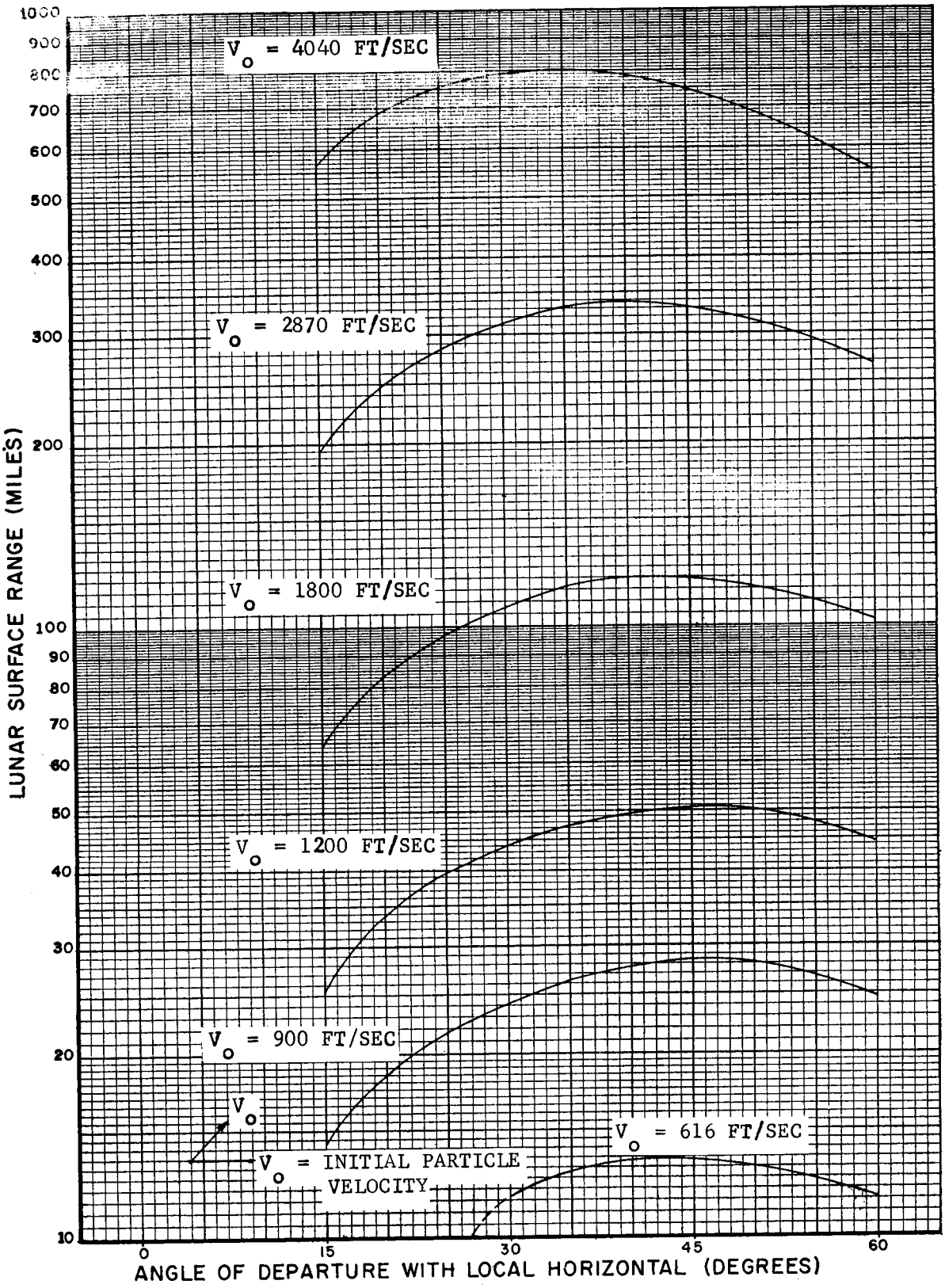

FIGURE 4. PARTICLE RANGE VERSUS ANGLE OF DEPARTURE
V_o < CIRCULAR ORBITAL VELOCITY

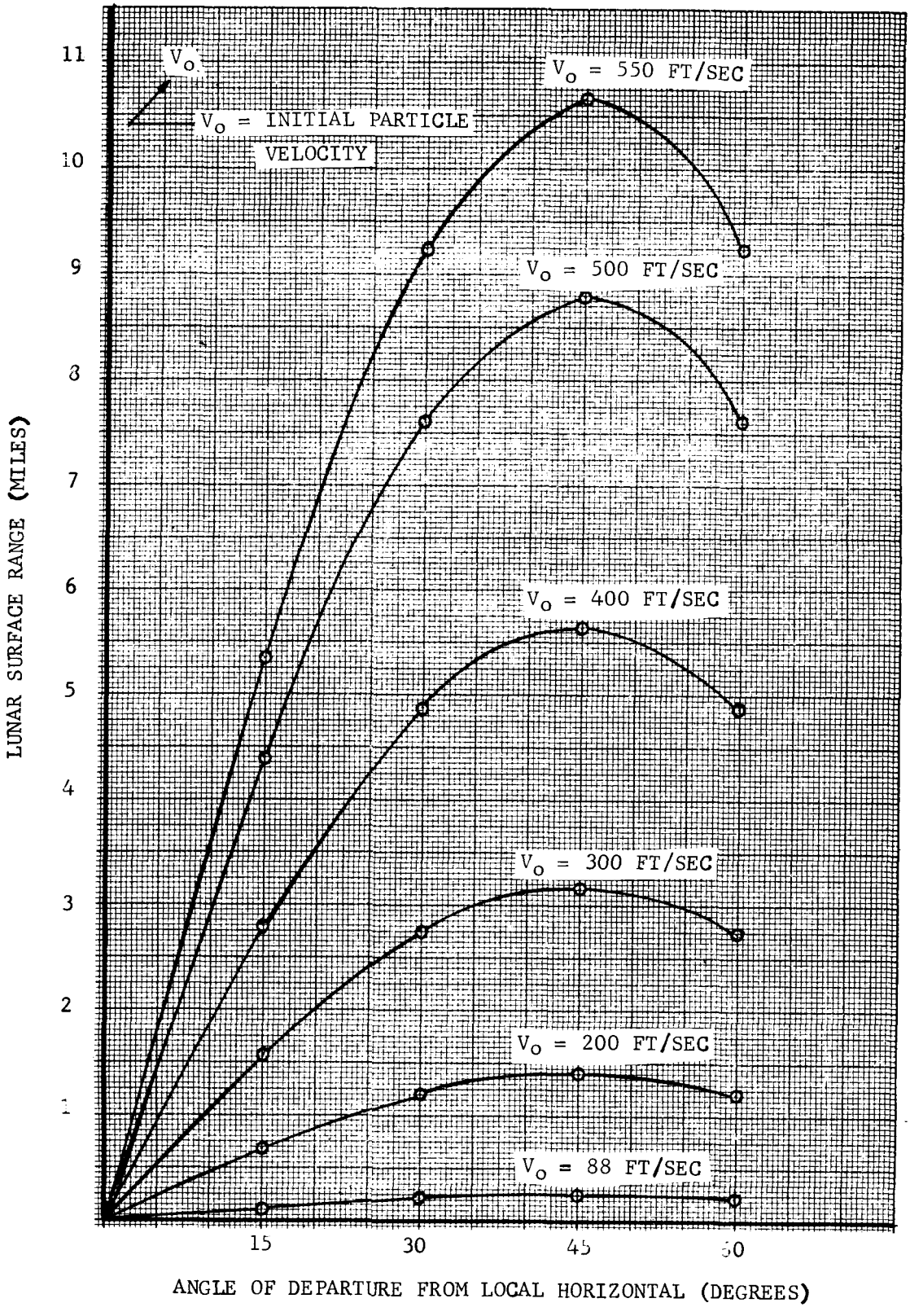

FIGURE 5. PARTICLE RANGE VERSUS ANGLE OF DEPARTURE
V_o < CIRCULAR ORBITAL VELOCITY

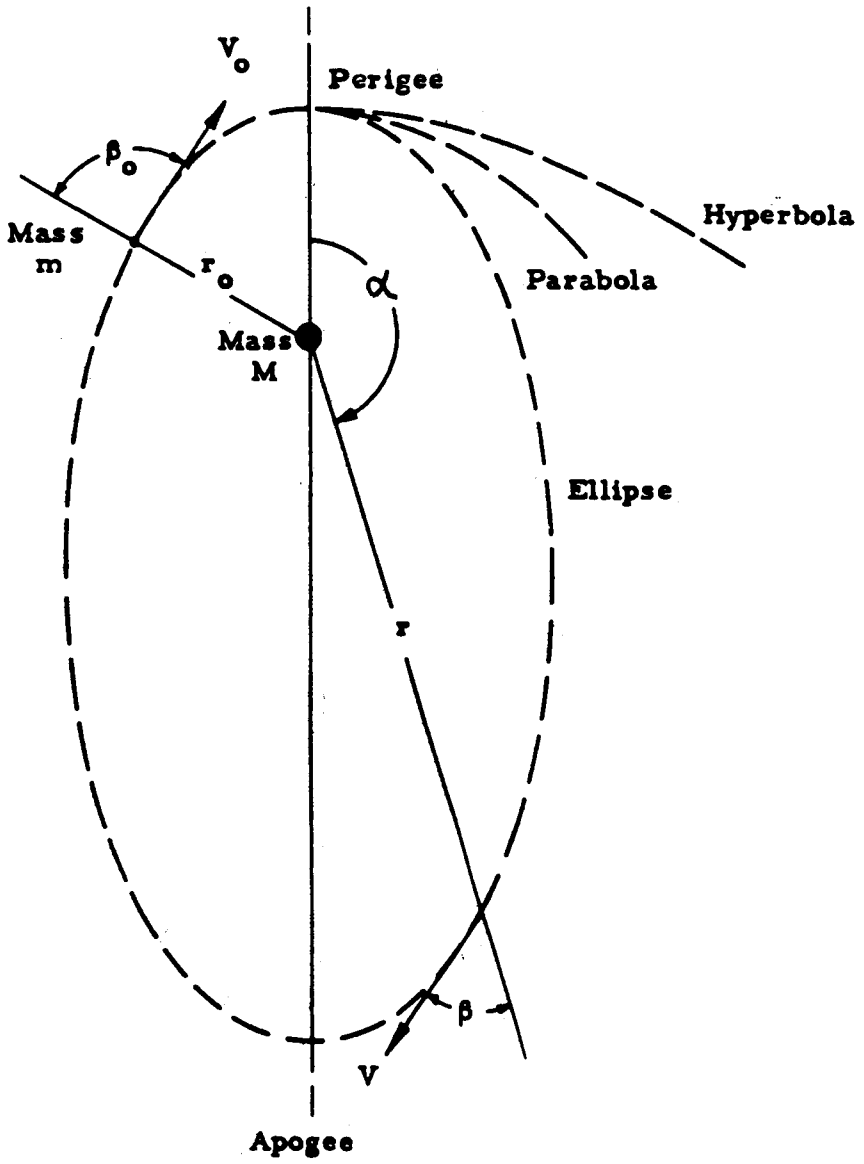

$$\lambda = \frac{V_o^2 r_o}{GM} \quad ; \quad \lambda < 2 \text{ Elliptical Path}$$

$\lambda = 1$ Circular Path ($\beta_o = 90^\circ$)

$\lambda = 2$ Parabolic Path

$\lambda > 2$ Hyperbolic Path

$$\text{Eccentricity } e = \sqrt{1-\lambda(2-\lambda)\sin^2\beta_o}$$

$$\text{Perigee Distance } r_{min} = \left(\frac{1-e}{2-\lambda}\right) r_o$$

$$\text{Apogee Distance } r_{max} = \left(\frac{1+e}{2-\lambda}\right) r_o$$

$$\text{Period } T = \frac{2\pi\left(\frac{r_o}{2-\lambda}\right)^{3/2}}{\sqrt{GM}}$$

$$\text{Velocity } V = V_o\sqrt{1+\frac{2}{\lambda}\left(\frac{r_o}{r}-1\right)}$$

$$\text{Angle } \alpha = \cos^{-1}\frac{1}{e}\left[\left(\frac{1-e^2}{2-\lambda}\right)\frac{r_o}{r}-1\right]$$

FIGURE 6. MOTION OF A PARTICLE IN A CENTRAL FORCE FIELD OF INVERSE SQUARE INTENSITY

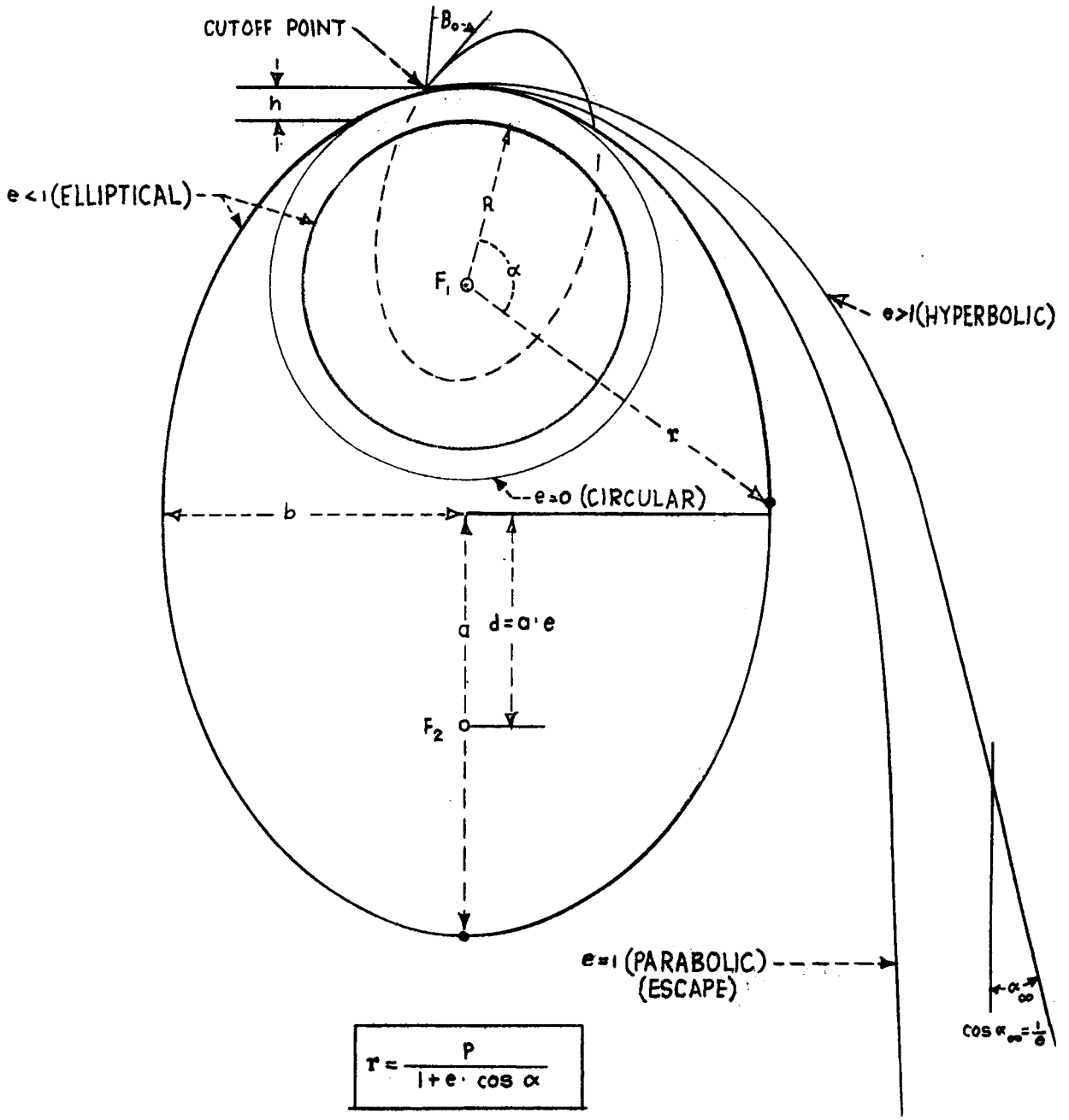

FIGURE 7. INERTIAL TRAJECTORIES IN A CENTRAL GRAVITY FIELD

REFERENCES AND BIBLIOGRAPHY

1. Fried, B. D. and Richardson, J. M., Optimum Rocket Trajectories, Journal of Applied Physics, Vol. 27, No. 8, August, 1956.

2. CEX 58.9 Civil Effects Study, A Model Designed to Predict the Motion of Objects Translated by Classical Blast Waves, June 29, 1961, U. S. AEC.

3. Hymer, Glen and Vann, J. W., R&D Division, Redstone Arsenal, Exhaust Blast Pressures of Rockets, Report 353N4, June 7, 1956, CONFIDENTIAL.

4. Stitt, Leonard E., Interaction of Highly Underexpanded Jets with Simulated Lunar Surfaces, Lewis Research Center, Cleveland, Ohio, NASA TN D-1095, December, 1961.

5. Moulton, Celestial Mechanics, 2nd revised edition - 1959, The McMillan Co.

6. Dergarabedian, Paul, Missile Performance, University of California Space Technology Laboratories, Ballistic and Space Vehicle Systems, UCLA Film Series, X431.

7. Fundamental Flight Dynamics and Staging, Summary for UCLA Film Series Course X431DEF.

8. Missions and Vehicle Design, UCLA Film Series Course X431DEF.

9. Mickelwait, A. B., Flight Dynamics, UCLA Film Series Course X431DEF, Lecture 8.

10. Effects of Rocket Jets on Surrounding Areas, White Sands Proving Ground, TM #9, July 18, 1962, CONFIDENTIAL.

11. Effects of Rocket Exhaust on Launching Areas, Engineering Labs, Corps of Engineers Report 1430, Project 8-17-02-001, October 25, 1955, CONFIDENTIAL.

12. Rocket Blast Effect Program, John Hopkins University, Contract Nord 7386, Bureau of Ordnance, U. S. Navy, Report CM-747, August 6, 1952, SECRET.

13. Operation Plumbbob, Project 33.3 Tertiary Effects of Blast, Displacement DASAWT 1469, May 22, 1959, Civil Effects Test Group.

14. Shapiro, Ascher, H., The Dynamics and Thermodynamics of Compressible Fluid Flow, vol I, The Ronald Press Co., New York, N. Y.

NASA-Langley, 1963